Optimal cell transport in straight channels and networks

Alexander Farutin, Zaiyi Shen, Gaël Prado, Vassanti Audemar, Hamid Ez-Zahraouy, Abdelilah Benyoussef, Benoit Polack, Jens Harting, Petia M Vlahovska, Thomas Podgorski, et al.

Optimal cell transport in straight channels and networks

Alexander Farutin,[1,2] Zaiyi Shen,[1,2] Gael Prado,[1,2] Vassanti Audemar,[1,2] Hamid Ez-Zahraouy,[3] Abdelilah Benyoussef,[3] Benoit Polack,[4,5] Jens Harting,[6,7,8] Petia M. Vlahovska,[9] Thomas Podgorski,[1,2] Gwennou Coupier,[1,2,*] and Chaouqi Misbah[1,2,†]

[1]*Université Grenoble Alpes, LIPHY, F-38000 Grenoble, France*

[2]*CNRS, LIPHY, F-38000 Grenoble, France*

[3]*Laboratoire de Matière Condensée et Sciences Interdisciplinaires, Faculty of Sciences, Mohammed V University of Rabat, 10000 Morocco*

[4]*Laboratoire d'Hématologie, CHU, F-38000 Grenoble, France*

[5]*TIMC-IMAG/TheREx, CNRS UMR5525, Université Grenoble Alpes, F-38000 Grenoble, France*

[6]*Helmholtz Institute Erlangen-Nürnberg for Renewable Energy (IEK-11), Forschungszentrum Jülich, Fürther Strasse 248, 90429 Nürnberg, Germany*

[7]*Department of Applied Physics, Eindhoven University of Technology, P.O. Box 513, 5600MB Eindhoven, The Netherlands*

[8]*Faculty of Science and Technology, Mesa+ Institute, University of Twente, 7500 AE Enschede, The Netherlands*

[9]*Engineering Sciences and Applied Math, Northwestern University, Evanston, Illinois 60208, USA*

(Received 4 May 2018; published 11 October 2018)

Flux of rigid or soft particles (such as drops, vesicles, red blood cells, etc.) in a channel is a complex function of particle concentration, which depends on the details of induced dissipation and suspension structure due to hydrodynamic interactions with walls or between neighboring particles. Through two-dimensional and three-dimensional simulations and a simple model that reveals the contribution of the main characteristics of the flowing suspension, we discuss the existence of an optimal volume fraction for cell transport and its dependence on the cell mechanical properties. The example of blood is explored in detail, by adopting the commonly used modeling of red blood cells dynamics. We highlight the complexity of optimization at the level of a network, due to the antagonist evolution of local volume fraction and optimal volume fraction with the channels diameter. In the case of the blood network, the most recent results on the size evolution of vessels along the circulatory network of healthy organs suggest that the red blood cell volume fraction (hematocrit) of healthy subjects is close to optimality, as far as transport only is concerned. However, the hematocrit value of patients suffering from diverse red blood cel pathologies may strongly deviate from optimality.

DOI: 10.1103/PhysRevFluids.3.103603

I. INTRODUCTION

Lab-on-a-chip technologies allow for high throughput analysis or manipulation at the level of single particles, in particular biological cells or droplets. They are now part of the scientific and industrial landscape. While most concepts have been initially developed on dilute suspensions, the possibility of manipulating more concentrated suspensions is now explored [1–3]. The expected

*gwennou.coupier@univ-grenoble-alpes.fr

†chaouqi.misbah@univ-grenoble-alpes.fr

gains in throughput have to be evaluated in light of the potential decrease of the process efficiency, due to cell-cell interactions [4], screening of the controlling external field (e.g., in acoustophoresis [3]), etc. In addition, substantially increasing particle concentration will eventually lead to an increase of the viscosity which will often lead to a decrease in the particle flux, far before nonreversible events like clogging occur [5].

This points to the question of the existence or not of an optimal volume fraction of particles that would optimize their transport for given boundary conditions like pressure difference at the inlet and outlet of a channel network, as considered here.

This question naturally arises also in blood vascular networks which have a complex architecture, and where oxygen is delivered to tissues via the red blood cell (RBC) hemoglobin. About 40%–45% of blood volume is composed of RBCs (in the macrocirculation). Given its medical importance, e.g., in blood transfusion, the existence of an optimal hematocrit (optimal volume percentage of RBCs) has been extensively discussed in the physiology and hemorheology literature [6–13].

Optimality in living systems is a subtle question to be tackled with care. In addition to oxygen transport, blood has many other biological functions such as thermoregulation, lymph production, immune response, or carbon dioxide, nutrients, and waste transport. Yet, it is still worth asking whether RBC transport (and as a corollary oxygen transport) is optimum or not and, more importantly, what is the impact of cell mechanical properties or network architecture characteristics on optimal transport. Understanding these questions may help understanding situations of hypoxia in relation with pathological evolution of these parameters, or provide hints toward developing artificial blood.

In this paper, we consider blood as a reference example. We shall first explore the impact of variations in the properties of red blood cells on the overall transport property (cell flow rate). More precisely, we investigate the role of cell mechanical properties, that of reduced volume—more or less deflated cell—with incompressible membrane, as well as the role of membrane (the case of capsules). In a second part, we will analyze the effect of network geometry on the cell flow rate. Finite-size effects of the cells plus the existence of cross-stream migration (lift) of hydrodynamic origin generally lead to nonuniform distribution of the flowing particles [14–18], which in turn leads to a decrease of volume fractions in smaller channels (called the Fåhræus effect for blood [19,20]), and uneven distribution of cells in a network of small channels, due to peculiar phase separation effects at the level of bifurcations [21–24]. This points to the fact that a global optimality at the level of a network is probably not the consequence of an optimization at each level, but most likely as a nonlocal compromise involving different levels of vessel branches.

In the case of blood flow, we find that optimality cannot be reached in all the vessels of the circulatory system at the same time. For straight channels it is found that the optimal hematocrit (RBC volume fraction) matches the actual hematocrit in large arterioles, in the range 100–200 μm (for humans the arteriole range is 10–200 μm [25]). For a vessel network (mimicking the real vasculature), we find that the cell flux is dominated by these arterioles and larger vessels, and that the hematocrit (as defined in routine blood tests) of a healthy subject is close to optimality.

Solving blood distribution problems *in silico* is challenging and highly nontrivial because of the complex nature of blood flow: it involves many deformable RBCs moving and interacting in blood vessels with complicated geometry [26–30]. Recent advances in computational power and novel simulation approaches, however, are beginning to make the task tractable and the bottom-up simulations of blood flow (by explicitly accounting for blood elements) are becoming realistic [30]. Computational approaches based on continuum formulations [17,31–43] or particle-based models [44–50] have been successfully applied to simulations of the flow of single and many RBCs. These simulations have revealed that many phenomena in blood flow such as platelet and leukocyte margination, plasma skimming, and clustering [17,20,51–55] have a purely mechanistic origin. For example, plasma skimming and hematocrit decrease in the microcirculation (Fåhræus effect) [20] arise from a cross-streamline migration of RBCs due to local flow perturbation by the deformable RBCs [32,56,57]. Many experiments have pointed to and continue to reveal a plethora of effects on the individual and collective behaviors of RBCs under flow [23,28,58–61].

We investigate stationary blood flow properties using both numerical simulations and analytical studies covering a wide volume fraction range. While in the arterioles the pulsatile nature of flow has not been fully damped yet, the associated Womersley number is of order 0.05 [62]; therefore at each moment the velocity profile is similar to that of the stationary case. In the simulations we use two models for cells: (i) a three-dimensional (3D) model accounting for both bending energy and in-plane shear elasticity, and solved by the lattice Boltzmann method (LBM). This 3D model will be also used to consider capsules with extensible membranes, while RBC ones are not; (ii) a two-dimensional (2D) model based on the LBM which accounts for membrane bending elasticity that shows the same trends, offering a faster tool to explore wider ranges of parameters. These simulations are completed by a discussion based on a simple model that incorporates the most important features of the rheology and structure of a suspension, which can be used to anticipate the impact of the variations of cell or network parameters.

II. MATERIALS AND METHODS

We represent cells as either a contour endowed with bending energy immersed in a 2D fluid, or as a surface having both bending energy and shear elasticity in a 3D fluid. The simulation uses a 2D [48] and 3D [63] lattice Boltzmann method. The bending energy is given by $E = (\kappa/2)\int H^2 dA$ with H the mean curvature, dA the arclength in 2D or area in 3D, and κ the bending rigidity modulus. In 3D, the membrane has additionally a shear elastic energy written as $\mu_s(I_1^2 + 2I_1 - I_2)/12 + \kappa_\alpha I_2^2/12$, where μ_s is the shear elastic modulus and κ_α is the area dilation modulus. I_1 and I_2 are the in-plane strain invariants (see [63]).

We impose a pressure difference Δp between the inlet and outlet of a straight channel of length L and width W for several values of volume fraction Φ_t. The channel widths range from $W = 2R$, where R is the cell effective radius, up to $W = 64R$, thus covering the range of *in vitro* applications and the capillary to arteriole scale for the blood network. In the absence of cells the flow is of a Poiseuille type. Periodic boundary conditions are considered in the longitudinal direction and also in the third direction in 3D. In 2D (3D) the volume fraction in the channel, called tube volume fraction Φ_t, is defined as $\Phi_t = NA/\mathscr{A}$ $(NV/\mathscr{V})$ where N is the number of cells in the channel, A the area of the cell, and V the volume, whereas $\mathscr{A}$ and $\mathscr{V}$ designate the total area and volume of the channel. η is taken as 1.2 m Pa s (plasma viscosity), and the enclosed fluid within cells is taken to have the same viscosity. The precise values of the viscosity contrast have little influence on the results, as shown below. We define the capillary numbers (which are a measure of the flow strength over the cells mechanical resistance) associated with bending and shear elastic modes as $C_a = \eta\langle\dot\gamma\rangle R^3/\kappa$ and $C_s = \eta\langle\dot\gamma\rangle R/\mu_s$, with $\langle\dot\gamma\rangle = 2U_{\max}/W$, where $U_{\max}$ is the maximum velocity in the channel in the absence of cells. As a reference, we have taken $\kappa \simeq 3\times10^{-19}$ J and $\mu_s \simeq 4$ μN/m, close to that known for RBCs [64]. We define in 2D $R = \sqrt{A/\pi}$, and in 3D $R = [3V/(4\pi)]^{1/3}$ as the typical cell radius. For a healthy RBC we have $R \simeq 2.7$ μm.

We will explore values from 0.09 to 90 for C_a in 2D and from 0.2 to 0.9 for C_s in 3D. This latter range corresponds to that found for red blood cells, considering typical vessel diameters of human capillaries and arterioles (about 5–10 μm and 10–200 μm, respectively [25]) and typical maximal velocities in capillaries and arterioles (1–10 mm/s) [65].

We define (in 2D) the reduced area $\nu_{2D} \equiv (A/\pi)/(p/2\pi)^2$ (with p the perimeter and A the enclosed area) and the reduced volume (in 3D) $\nu \equiv [V/(4\pi/3)]/[A/4\pi]^{3/2}$. For a healthy RBC, ν is reported to be in the range $\simeq$0.6–0.64 [66,67]. Here, we chose as a reference $\nu = 0.64$, as in other simulation papers of the literature [30,61,68]. Higher values will also be explored. For blood, several diseases (spherocytosis, ellipsocytosis) correspond to the high value of ν, close to 1. $\nu = 1$ plus an incompressible membrane also corresponds to the case of a suspension of hard spheres. In 2D, we choose $\nu_{2D} = 0.7$, which is the reduced area of the section along the main axis of a prolate spheroid of reduced volume 0.6.

Finally, we varied κ_α/μ_s between 1.25 and 125 to explore the effect of area dilation. The value 125 is our reference case and is large enough to preserve the membrane area locally and corresponds

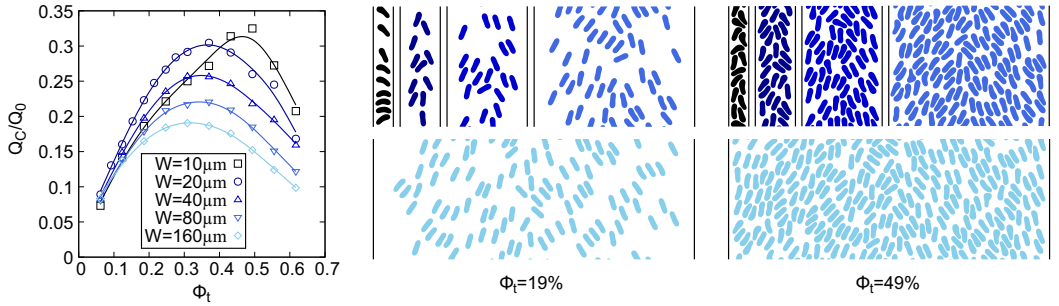

FIG. 1. (2D simulations) Left panel: Normalized cell flow rate as a function of volume fraction for channels with different widths. Full lines are a guide for the eyes. $C_a = 0.9$ and the reduced area is $\nu_{2D} = 0.7$. Center and right panels: snapshots of the suspension for two different volume fractions in the five considered channels.

to red blood cells, while lower values allow one to consider the case of what is usually called elastic capsules.

III. OPTIMAL FLUX IN A STRAIGHT CHANNEL

Throughout the paper, we focus on the cell flow rate Q_C normalized by the flow rate of the cell-free fluid Q_0 under the same pressure gradient. In the simulations, the flow rate Q_C is calculated by counting the number of cells that cross a given section in the channel, averaged over long runs.

A. Simulation results

a. Role of flow characteristics. We investigate first the effect of flow strength (measured by the capillary number) and channel width. These simulations are performed in 2D.

Figure 1 shows that Q_C/Q_0 exhibits a maximum as a function of volume fraction Φ_t. It illustrates the effect of channel width on the corresponding optimal volume fraction Φ_o. The results show that Φ_o varies between 0.3 in large enough channels ($W = 160\ \mu$m) to about 0.4 in smaller channels ($W = 10\ \mu$m). The corresponding cell flux also increases when the channel gets narrower. This shift of the cell flow rate curves is related to the increase of the effective viscosity with the channel diameter. This effect is known for blood as the Fåhræus-Lindquist effect [20]. It stems from the fact that the thickness of the cell-free layer near the walls depends only weakly on the channel diameter, as it is essentially the result of local interactions. Therefore, the relative contribution of this low-viscosity layer to the effective viscosity of the whole fluid becomes less and less important as the channel diameter increases.

Figure 2 shows that the maximum of Q_C/Q_0 is quite sensitive to the flow strength C_a: the optimal volume fraction Φ_o increases from 0.3 to more than 0.4 over three orders of magnitude of increase in C_a. The corresponding cell flux increases in the same proportion. These results can be considered as a consequence of the increased cell deformation that makes the suspension less viscous (shear thinning behavior).

b. Role of cell properties. We now turn to the effect of modifications of the cell properties, which is explored through 3D simulations. Figure 3 shows that a spherical shape of the cells lowers both the optimal Φ_o and the maximum cell flow rate. For example, when the reduced volume ν passes from 0.64 to 0.99 the maximal carrying capacity drops by about 25%. This is attributed to the fact that cells are less deformable because of the nearly spherical shape reducing their ability to squeeze and accommodate high Φ_t. Moreover, cross-stream migration is suppressed and the cell-free layer diminishes, leading to increased flow resistance.

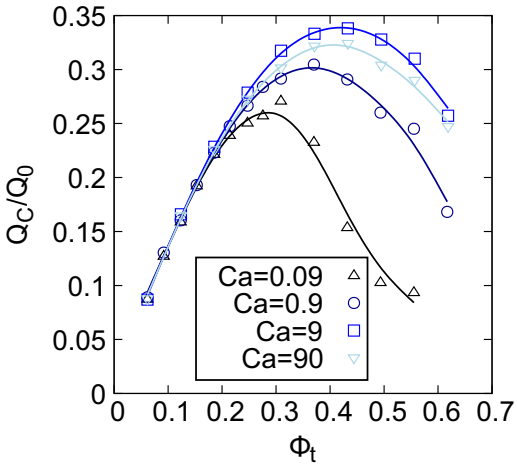

FIG. 2. (2D simulations) Normalized cell flow rate as a function of volume fraction for a channel width $W = 20\ \mu$m and different C_a. Reduced area is $\nu_{2D} = 0.7$.

When membranes are incompressible, reduced volume determines the ability of cells to deform. This ability can also be lost by an alteration of the mechanical property (e.g., shear elasticity) of the membrane. For example, in sickle cell and malaria diseases, the RBC elastic modulus can be significantly higher (up to about three times higher [64]) than within healthy subjects. An increase of the elastic modulus is equivalent to a decrease of the capillary number. Our data in Fig. 2 show that a reduction of the capillary number leads to a significant decrease of the cell flow rate.

The role of membrane compressional elasticity on the maximum cell flow rate is explored in Fig. 4. The green data correspond to incompressible membranes. To explore the effect of variations of the area dilation modulus κ_α (violet data), we have selected an initial reduced volume $\nu = 1$ (the same for all cells) and performed several simulations, each time with different elastic properties (κ_α/μ_s between 1.25 and 125). Each cell within the same uniform suspension (i.e., all cells have the same properties) experiences different shear stress and thus will be more or less stretched. The average actual reduced volume within the suspension is shown as a filled square, whereas the horizontal bars show the distribution of reduced volume for each simulation (i.e., for a given stretching elastic coefficient). One sees that a moderate extensibility $\kappa_\alpha/\mu_s \approx 1.25$, allowing an

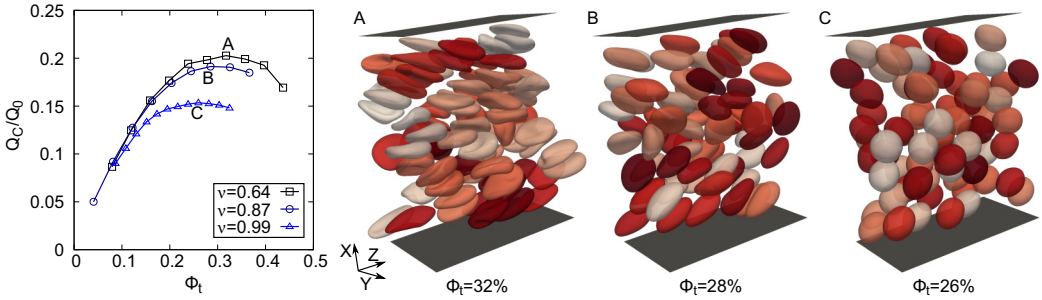

FIG. 3. (3D simulations) Left: The normalized cell flow rate as a function of tube volume fraction Φ_t for different reduced volumes. Viscosity contrast is 1 and the channel width W is 40 μm $= 14.8R$; the channel length along the flow direction is about $11.7R$, and is equal to $6.2R$ in the orthogonal direction. $C_s = 0.18$. A, B, and C are snapshots of suspension configurations for the three different reduced volumes shown for the corresponding optimal volume fraction.

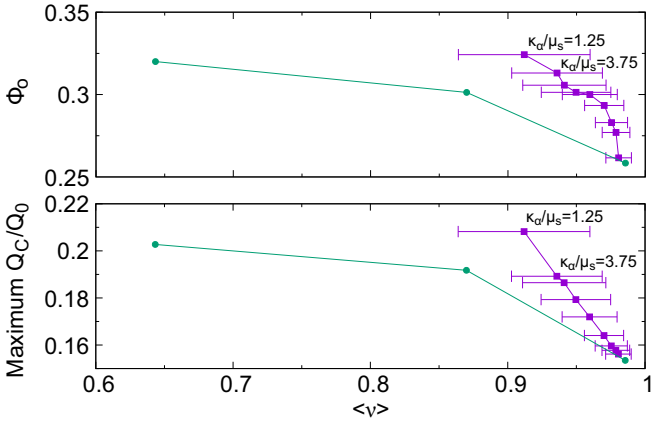

FIG. 4. (3D simulations) Green line: Optimal flux and optimal volume fraction as a function of the actual reduced volume (3D simulations) for incompressible membranes (from Fig. 3). Violet lines: the same simulation with stretchable capsules. For each simulation the compressional elasticity κ_α/μ_s has been varied in order to allow for different average reduced volume $\langle v \rangle$. Each capsule experiences different shear stresses within the channel, and thus has a different surface area (and thus reduced volume); the horizontal bars provide the distribution width of reduced volumes within the same suspension. $C_s = 0.18$, as in Fig. 3.

average decrease of the reduced volume of the capsules from $\langle v \rangle = 1$ to ≈ 0.9, leads to a maximum flow rate $\max(Q_C/Q_0) \approx 0.2$ equivalent to that of healthy incompressible red blood cells, even though the capsules are quasispherical. Interestingly, the cell flow rate is more important for stretchable capsules than for nonstretchable cells having the same reduced volume. The ability to deform leads to better accommodation to the flow stress, with different shapes within the suspension.

B. Analytical model

We develop an analytical model that captures the computational observations for the dependence of Q_C on tube volume fraction Φ_t. This analytical model provides a means for a quick estimate of the optimal volume fraction and insight into the mechanisms that control the phenomenon, as explored by our simulations. We adopt a continuous two-fluid model for suspension flow. Such an approach has already proved to give interesting insights for other problems related to blood flow [69–71]. Here, we consider an inner core containing a homogeneous suspension of volume fraction Φ surrounded by a cell-free layer of thickness e, flowing in a tube of radius $R_0 = W/2$. For given tube volume fraction Φ_t, $\Phi = \Phi_t(\frac{R_0}{R_0-e})^2$.

The cell flux is

$$Q_C(\Phi_t) = \Phi \int_0^{R_0-e} v(\Phi, r) 2\pi r dr, \tag{1}$$

and the total flux is given by

$$Q_T(\Phi) = \int_0^{R_0} v(\Phi, r) 2\pi r dr. \tag{2}$$

For a given pressure gradient (flow strength), the Stokes velocity profiles $v(\Phi, r)$ in the outer cell-free annulus and in the core can be evaluated. Assuming that the core fluid is a homogeneous, dense suspension of concentration Φ, its relative viscosity $\bar{\eta} \equiv \eta(\Phi)/\eta_0$ can be estimated from the Krieger-Dougherty law $\bar{\eta} = (1 - \Phi/\Phi_m)^{-[\eta]\Phi_m}$, where Φ_m is the maximum fraction, $[\eta]$ is the intrinsic viscosity, and η_0 is the viscosity of the cell-free fluid [72]. This law was chosen since it is simple enough to allow discussion on how it should evolve with the cell properties, but accurate

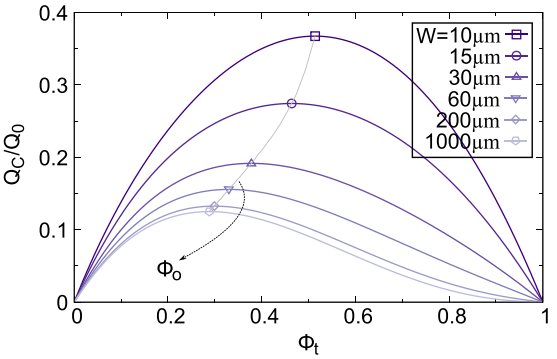

FIG. 5. The particle flow rate as a function of tube volume fraction for channels with different diameter calculated from our minimal model. We took $e_0 = 2\ \mu$m, $[\eta] = 5/2$ as for rigid spheres and for RBCs in physiological conditions [78], and Φ_m is chosen as equal to 1 considering that the cells are deformable and can be squeezed.

enough to describe viscosity evolution with cell concentration: the Quemada law, a particular case of Krieger-Dougherty law, describes well the bulk behavior of blood [71]. To first order, e is independent of w, at least for $w > 15$ μm [73], and is mainly determined by the balance between the lift flux and the diffusive flux. This can be seen in the central and right panels of Fig. 1. Due to the linear relationship between the diffusion constant and local volume fraction [60,74], we assume that the thickness of the outer cell-free layer decreases linearly as volume fraction increases, an assumption which is validated in the literature [17,23,73]. Consequently, we set $e = e_0(1 - \Phi_t/\Phi_m)$ where e_0 is a constant characterizing the cell-free layer at low volume fraction. Strictly speaking, this model is not valid for very low fraction where e is expected to converge to $w/2$. Despite the oversimplification, this model captures the main features as long as we focus on large enough Φ so that hydrodynamic interactions among cells counterbalance the effect of walls. This is indeed the range where the optimal volume fraction is expected. Note that very few interaction events are sufficient to balance the lift force, because the latter strongly decreases with distance to the wall [60,75–77]. Finally,

$$\frac{Q_C}{Q_0} = \frac{Q_C}{Q_T(\Phi = 0)} = \frac{\Phi(R_0 - e)^2\left\{R_0^2 + [2\bar{\eta}(\Phi) - 1](2eR_0 - e^2)\right\}}{\bar{\eta}(\Phi)R_0^4}, \tag{3}$$

where e and Φ are the functions of Φ_t given above.

Figure 5 illustrates the prediction of this reduced model. As in simulations, it is seen that the optimal volume fraction increases with the confinement, and so does the corresponding cell flux. Had we assumed a fixed cell-free layer, independent of Φ_t, we would then have missed the fact (data not shown, already shown in Ref. [9]) that optimal volume fraction increases with confinement.

We now exploit further the results of this simplified model to help with proposing scenarios for the evolution of the optimal volume fraction with some cell or flow properties (see Fig. 6). The evolution of the optimal volume fraction with the reduced volume, seen in Fig. 4 (obtained numerically), can be understood by using our minimal model: if one considers less deflated cells, the intrinsic viscosity $[\eta]$ is not expected to vary too much since it is equal to 5/2 for spheres and close to that value for RBCs [78]. On the other hand, inflating cells leads to a decrease of the maximal packing fraction Φ_m, and to a decrease of the size of the cell-free layer e_0 [75,77,79]. Both effects lead to to a decrease of the optimal volume fraction and of the associated cell flux (Fig. 6, bottom and top panels), in agreement with Fig. 4.

Upon an increase of the capillary number, one expects the size of the cell-free layer to increase because of the increase of cell deformation and the resulting lift force [60], and the intrinsic viscosity to decrease, characterizing generic shear-thinning behavior of capsule suspensions. As seen in

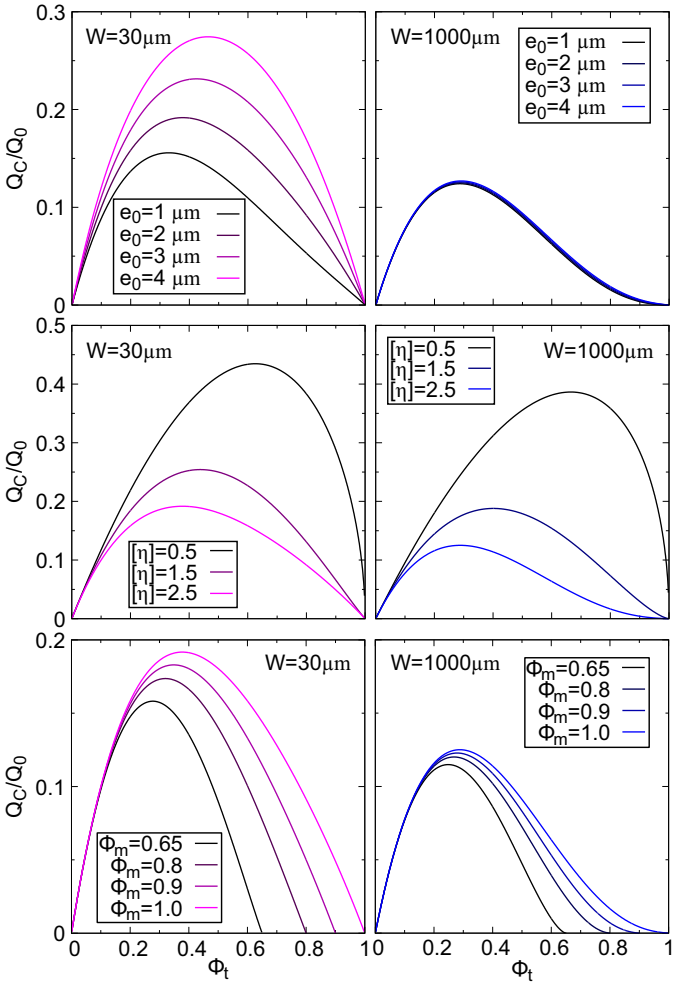

FIG. 6. RBC flux according to our minimal model. The reference configuration is $W = 30$ μm (left) or $W = 1000$ μm (right), $e_0 = 2$ μm, $[\eta] = 5/2$, and $\Phi_m = 1$. Top panel: e_0 is varied; middle panel: $[\eta]$ is varied; bottom panel: Φ_m is varied.

Fig. 6, top and middle panels, both effects lead to an increase of the optimal volume fraction, in agreement with Fig. 2.

Another situation which is classically explored in the literature regarding RBC deformation is to act on the viscosity of the suspending fluid [23,59,60,78,80]. By increasing the external viscosity the lift forces are expected to increase [60,81], hence the cell-free layer thickness also increases [23]. The impact on the rheology is less trivial. Contrary to drops for which the intrinsic viscosity is a monotonous function of external viscosity, the subtle interplay between inner fluid dynamics and the deformations allowed by the presence of the membrane lead to a nonmonotonous function in the case of cells with membranes [78,82]. Both for structuring [23] and for rheology [83] effects, the effect of decreased external viscosity is strongly reduced by a concentration increase. In particular, cells that would tumble in a dilute suspension tends to tank-tread when the cell concentration increases, as they would do in a more viscous suspending fluid. All in all, we can see in Fig. 7, that our 2D simulations show that in reality the flux does not depend much on the viscosity ratio between the inner and the outer fluid.

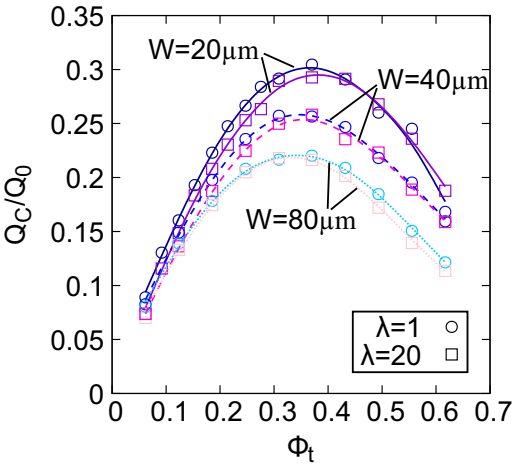

FIG. 7. (2D simulations) Normalized cell flow rate as a function of volume fraction for channels with different widths and two different viscosity ratios λ between the inner fluid and the external fluid. $C_a = 0.9$ and reduced area is $\nu_{2D} = 0.7$.

IV. OPTIMAL FLUX IN A NETWORK

The preceding results can be used to infer the flux of particles in a network. However, one must keep in mind that volume fraction is in general not a conserved quantity in a network (say from one branch of the network to another), or even in a straight tube of varying section. As a preliminary, we discuss this point first before presenting our results of flow rate in a network.

A. Tube and reservoir volume fraction

Starting from a large reservoir filled with a suspension of volume fraction Φ_r, one generally observes that the fraction decreases once the suspension enters a smaller channel. This effect, which is called the Fåhræus effect [19] for blood, results from the tendency of cells to accumulate in the center of the vessel (due to the wall-induced migration), acquiring thus a higher mean velocity than that of the suspending fluid and leading to a diluted flow in small channels: $\Phi_t < \Phi_r$. By contrast, in large channels, the relative effect of the wall-induced migration is negligible and the cells are homogeneously distributed within the channel section, implying $\Phi_t \simeq \Phi_r$.

By considering the conservation of particle flux, the reservoir volume fraction can be calculated from the results of a simulation or of the minimal model in a given tube: if $\langle V_C \rangle$ denotes the mean velocity of cells and $\langle V_T \rangle$ that of the whole suspension (cells plus the suspending fluid) in the tube, the total flow rate of cells across a section A of the tube is given by $Q_C = \langle V_C \rangle A \Phi_t$ and that of the whole suspension is given by $Q_T = \langle V_T \rangle A$. The ratio of Q_C to Q_T provides the volume fraction of cells found at the entrance or at the exit, Φ_r. We have thus the following relation:

$$\Phi_r = \frac{Q_C}{Q_T} = \Phi_t \frac{\langle V_C \rangle}{\langle V_T \rangle}. \tag{4}$$

In Fig. 8 the Φ_t values for $\Phi_r = 0.45$ are indicated for our minimal model, and one clearly sees first that the discrepancy between Φ_t and Φ_r increases with the confinement, and second that in a network fed by a given value of Φ_r, the flux can be suboptimal in some branches and superoptimal in others.

This is true also in the vascular network: Pries *et al.* considered in Ref. [52] a fit of experimental data to proposean empirical relationship between the effective viscosity of blood in a cylindrical tube of diameter W and the tube hematocrit (=volume fraction in red blood cells) Φ_t, as well as

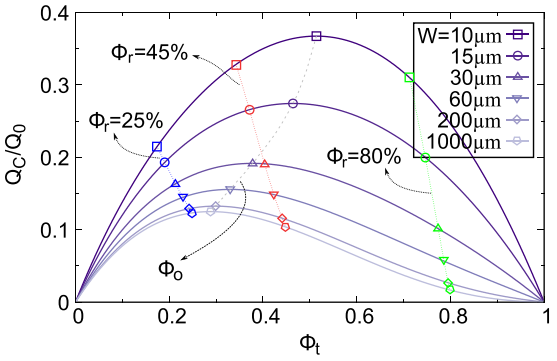

FIG. 8. The particle flow rate as a function of tube volume fraction from our minimal model (same data as in Fig. 5). In addition, the red line indicates the Φ_t value corresponding to a reservoir volume fraction Φ_r of 45% for the corresponding model. Blue and green lines correspond to high Φ_r (80%) and low Φ_r (25%).

between this tube hematocrit and the reservoir hematocrit Φ_r. Both functions $\eta_p(\Phi_t)$ and $\Phi_r(\Phi_t)$ are given in [52]. The relative RBC flow rate at constant pressure drop is then given by $Q_C/Q_0 = \Phi_r(\Phi_t)\frac{\eta_p(\Phi_t=0)}{\eta_p(\Phi_t)}$.

Figure 9 shows this relative RBC flow rate as a function of the tube hematocrit for different channel diameters. The existence of an optimal hematocrit is highlighted, which increases with the confinement. The same holds for the maximum RBC flow rate. Note that the value of this maximum as well as its position are well captured by our minimal model (Fig. 5).

The usually referenced hematocrits, measured in medical blood tests, are in the ranges 0.34–0.45 and 0.39–0.49 for women and men, respectively [84], and correspond to values encountered in macrocirculation. The red points in Fig. 9 show the tube hematocrit that would result from the $\Phi_r = 0.45$ reservoir (systemic) hematocrit.

Patients suffering from a low or high level of hematocrit (anemia and polycythemia, respectively) are clearly far from optimality. Indeed, if the reservoir hematocrit is small enough ($\Phi_r = 0.25$), as happens in severe anemia disease (blue line in Fig. 9), or large enough ($\Phi_r = 0.8$) as is the case in polycythemia vera (green line in Fig. 9), then the tube hematocrit does not cross any optimal value when varying the tube diameter. In the anemia disease case the hematocrit remains suboptimal,

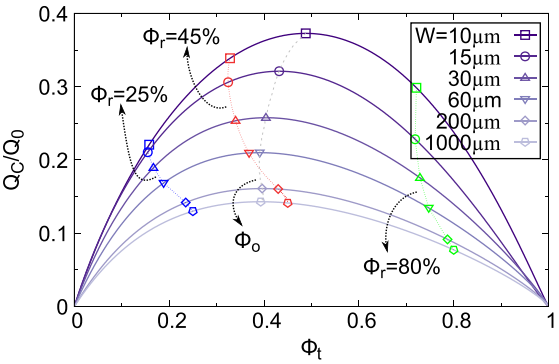

FIG. 9. The RBC flow rate as a function of the tube hematocrit for channels of different diameters calculated from Pries empirical model [52]. The red line indicates the Φ_t value corresponding to a reservoir hematocrit of 45%. Blue and green lines correspond to high Φ_r (80%, polycythemia) and low Φ_r (25%, anemia).

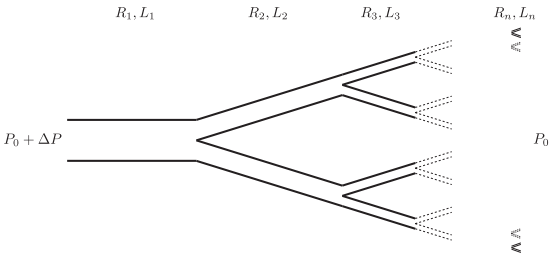

FIG. 10. Sketch of the model network considered in Sec. IV B.

while it remains superoptimal in the polycythemia disease. In the first case the attained maximal flow rate in arterioles is about 25% lower than in healthy subjects, while the situation is more severe in the second case where the reduction can attain about 60%.

Back to the healthy case, one notices that the tube hematocrit Φ_t corresponding to $\Phi_r = 45\%$ is optimal in large channels until $W = 60$ μm, which corresponds to the medium diameter range of human arterioles. This is interesting inasmuch as two-thirds of the oxygen is known to be delivered in the arteriolar trees [85] before reaching capillaries. On the contrary, in capillaries, the tube hematocrit is suboptimal for a reservoir hematocrit of 45%. This shows that optimality in a network can probably not be the result of local optimality everywhere in the network. The relative contribution of each branch to the overall particle flux must therefore be estimated.

B. Particle flux in a network

We consider a simplified network consisting of N levels enumerated as $i = 1 \ldots n$ (see Fig. 10). Level 1 consists of one straight cylindrical channel. Each channel of level i has radius R_i and length L_i. It divides symmetrically into two channels of level $i + 1$. At each step, the cell and plasma fluxes also split symmetrically, so that Φ_r is a conserved quantity [we recall that Φ_r is defined in Eq. (4) and is not to be confused with the actual hematocrit in a given branch of the network, which is the tube hematocrit]. We consider a fixed pressure drop ΔP between the inlet of the level-1 channel and the outlets of the level-n channels. Assuming bifurcation junctions do not contribute to pressure drop, one straightforwardly obtains

$$Q_C = \Phi_r Q_T = \Phi_r \Delta P \left\{ \sum_{i=1}^{n} 2^{-i+1} \frac{8 L_i \eta(\Phi_r, R_i)}{\pi R_i^4} \right\}^{-1}. \tag{5}$$

It is seen that the contribution of each channel depends on the detailed evolution of lengths and radii along the network. In addition, as already discussed, $\eta(\Phi_r, R_i)$ is generally an increasing function of R_i, therefore $\eta(\Phi_r, R_i)/R_i^4$ may depend on R_i in a complex way. We now illustrate this complexity for the case of blood flow.

Recently, the relationships between radii R_i and lengths L_i for living organisms have been discussed in detail using a statistical analysis based on 3D imaging in human subjects [86]. Adapted to our case of dichotomous and symmetric branching, these relationships can be written as $R_i^{1/a} = 2R(i+1)^{1/a}$ and $L_i^{1/b} = 2L(i+1)^{1/b}$, where a and b are exponents that can be extracted from fitting of *in vivo* data. Using the recursive formulas $R_i = 2^{-a(i-1)} R_1$ and $L_i = 2^{-b(i-1)} L_1$ we find

$$Q_C = \Phi_r \frac{\pi R_1^4 \Delta P}{8 L_1} \left\{ \sum_{i=1}^{n} 2^{(4a-b-1)(i-1)} \eta(\Phi_r, R_i) \right\}^{-1}. \tag{6}$$

The factor $2^{(4a-b-1)(i-1)}$ thus expresses the relative contribution from level i. According to [86], a value for a in the range 1/3–1/2 yields a good description of real data, with $a = 1/3$ for small

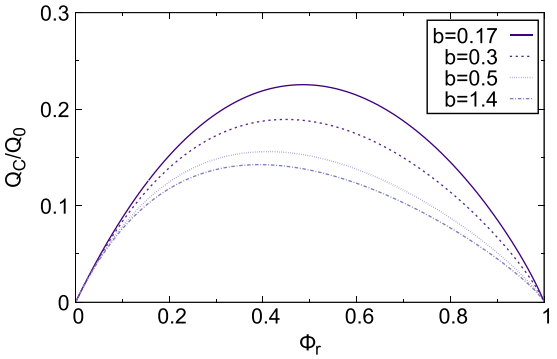

FIG. 11. The RBC flow rate as a function of the reservoir hematocrit for a model network (see text) for different values of b extracted from literature and empirical rheology law given in Ref. [52]. The curves are similar to those for large channels that would be obtained from Fig. 9 by considering Φ_r instead of Φ_t. Small values of b give more weight to the smallest vessels, hence an increase of the optimal hematocrit. Still, the contribution of large vessels is predominant.

vessels ($R_i < 1$ mm) and $a = 1/2$ for large vessels. An exponent-based scaling for the lengths is not as strongly supported by the data, since different measurements yield exponent b in the range 0.17–1.40. However, it is interesting to observe that for a and b within the aforementioned ranges, the exponent $4a - b - 1$ can be either negative or positive, indicating that the major contributions can come from large or from small vessels depending on the exponent sign. Since the effective viscosity significantly depends on the tube radius only when the radius is smaller than about 1 mm [52], we focus on the case $a = 1/3$, which is also consistent with Murray's law [87]. In that case, a realistic network geometry is likely to fall within a category where $4a - b - 1 = 1/3 - b < 0$ (since this is consistent with most available data for b), that is, a configuration where the flux would be regulated by large vessels.

In order to be more quantitative and include the dependency of the viscosity with the vessel radius, we consider in Fig. 11 a network starting from a channel of about 1 mm with successive bifurcations down to 5 μm, and plot the RBC flow rate as a function of reservoir hematocrit, as given by Eq. (6). Except for small b values, the curves are quantitatively closer to those obtained for large vessels than for small vessels (see Fig. 9), confirming that the dominant contribution arises from the largest vessels of the network. This would point to the fact that optimization of oxygen transport capacity may be regulated upstream of the microcirculation, close to the transition zone between small arteries and arterioles. Caution is, however, necessary since the situation is less clear for $a = 1/2$, for instance.

This result also implies that the optimal hematocrit Φ_0 is around known physiological values. However, given the dispersion of experimental data, the possibility for a positive exponent $4a - b - 1 = 1/3 - b$ is not to be excluded, in which case narrow channels would have more weight than larger vessels. A systematic analysis of the vessel size distribution in organs is needed before drawing more conclusive answers. In addition, the regularly branched network considered here is not the rule. For example, and as pointed out in Ref. [88], it has been shown that the network of vessels of a tumor, which grows much more rapidly than that of normal tissues, is chaotic and entangled, in contrast to the hierarchical branching pattern adopted here. More complex modeling for the geometry can be developed to account for this richness [89–91]. Handling this complexity and the different scales requires one to pay specific attention to the computational feasibility and accuracy, which may lead to the development of more complex flow models through specific assumptions which can be validated by our approach. For instance, in [91], the inhomogeneities and resulting nonlinearities due to complex cell partitioning in the capillary bed are explicitly neglected.

Indeed, while experimental studies of tube flow [11,19,92] yielded minimal values for the ratio Φ_t/Φ_r of about 0.7 for tubes of 20 and 10 μm diameters, in agreement with Pries law, *in vivo* studies [12,93,94] have shown that this ratio can fall in the range 0.3–0.5 in the microcirculation. These measurements have suggested that this is dependent on network topography and local flow rates. Asymmetric partitioning at the level of bifurcations can lead to important hematocrit variations between capillaries [53]. According to our network modeling, these variations should likely have no strong impact on the issue of optimization, as they occur in channels that are expected to play a minor role on the flux regulation. However, asymmetric partitioning of cells or asymmetry in the network geometry may have *a priori* an impact on the overall resistance of the capillary bed, and thus have a potential influence on optimality.

However, we expect this impact to be relatively small on the basis of the following argument. Let us consider two parallel branches originating from a bifurcation. We can calculate explicitly the effective resistance of this subnetwork by using Pries *et al.* viscosity law [52] and an adequate cell splitting model [95], which gives the cell flux ratio between the two branches as a function of their diameters ratio and the total flow rates ratio, in the case of upstream flow in stationary condition. If the mean diameter and the mean length between the two branches are kept constant and equal to the values given by the network scalings considered above, one finds that the resistance is always smaller than 110% of that of the symmetric case; note that in most cases, an even smaller value is found.

Cell splitting is controlled in a subtle way by the geometry and the rheology law, so that giving a simple intuitive argument about the overall behavior is not an easy task. However, some key features emerge from the following argument. First, we note that the conductance of the considered system is the sum of the conductances of the two branches. Conductance is proportional to the radius to the power 4, to the inverse of the branch length, and to the inverse of the viscosity, which is a quasilinear function of hematocrit in the range of interest. It is therefore a convex function of each of the three parameters (length, diameter, hematocrit) taken separately, which implies that any asymmetry in the cell splitting or in the geometry will mainly result in an increase of the conductance (and decrease of resistance and thus minor impact on optimality). Care must be taken, however. Since hematocrit repartition depends on the geometry, the different parameters are not independent and the convexity argument may not be entirely sufficient. Still it serves as a reasonable guideline.

Another point is worth being mentioned. In general, in a given branch of the microvasculature, the RBCs distribution may not be centered, by lack of long enough distance between two successive bifurcations; for instance, all cells may be close to one wall. In that case the partitioning will be quite different from the case of fully centered distribution, discussed above. For a given geometry, the convexity argument mentioned above clearly shows that the resistance will be lower than in the homogeneous distribution. Typically, it will be controlled by that of the branch that receives fewer cells.

This discussion suggests that even in nonidealized cases, the role of capillaries in the determination of the overall resistance and flux in a network is secondary compared to large vessels. Of course, detailed numerical simulations are necessary to fully conclude about the impact of asymmetries, beyond this simplified case of a two-branch network.

V. CONCLUSION

2D and 3D numerical simulations provided information on the behavior of cell flow rate as a function of cell volume fraction in a straight channel. Based on a minimal model we highlight the cell-free layer as a key element to understand the variation of the transport capacity of channels with diameter. This leads to the conclusion that the transport capacity of a whole network depends on its precise architecture, since two antagonist effects enter into play when traversing channels from large to small ones: (i) when the diameter of a channel decreases, the cell volume fraction decreases; (ii) at the same time, the value of the optimal cell volume fraction increases.

For red blood cells, the cell flux is directly linked to the oxygen transport capacity. Interestingly, the values obtained for the optimal hematocrit for vessel sizes corresponding to macrocirculation and intermediate microcirculation (arterioles) are close enough to the corresponding physiologically admitted values. Our analysis on a network where the weight of the contribution of each vessel has been extracted from *in vivo* data shows that this range of vessels also determines the RBC flow rate, indicating that the physiological values for the hematocrit are close to a kind of optimum in that sense. Our analysis also indicates the locations where active regulation processes like vasodilation or vasoconstriction are more likely to influence oxygen delivery.

Strong alterations are reported if the reduced volume of RBCs is increased, as is known for elliptocytosis and spherocytosis diseases. Not only is the flow rate of RBCs reduced in this case compared to the flow of healthy RBCs at the same hematocrit but also the optimal hematocrit is observed to be significantly lower. The lower value of RBC flow rate within patients suffering these diseases implies a severe collapse of oxygen delivery, which could lead to an increased heart load in order to maintain appropriate perfusion levels. It is known that elliptocytosis and spherocytosis diseases are accompanied by a reduction of the RBC count, a consequence of the spleen filtering. Interestingly, our results show that this decrease of hematocrit probably improves oxygen delivery.

We put forward here the idea that a slightly stretchable encapsulating membrane (like polymer-based capsules) would lead to a significant enhancement of oxygen transport capacity. The information generated by this study may guide the development of new soft materials, such as blood substitutes, and advance the tuning process and optimization of oxygen carriers. This study can also be adopted for more general questions of suspensions transport.

ACKNOWLEDGMENTS

This work was partially supported by CNES (Centre National d'Etudes Spatiales) and by the French-German university programme "Living Fluids" (Grant No. CFDA-Q1-14). C.M. thanks CNRST (project FINCOME).

[1] C. Wyatt Shields IV, C. D. Reyes, and G. P. Lopez, Microfluidic cell sorting: A review of the advances in the separation of cells from debulking to rare cell isolation, Lab Chip **15**, 1230 (2015).

[2] M. W. H. Ley and H. Bruus, Continuum modeling of hydrodynamic particle-particle interactions in microfluidic high-concentration suspensions, Lab Chip **16**, 1178 (2016).

[3] S. Karthick and A. K. Sen, Improved understanding of the acoustophoretic focusing of dense suspensions in a microchannel, Phys. Rev. E **96**, 052606 (2017).

[4] R. Vernekar and T. Krüger, Breakdown of deterministic lateral displacement efficiency for non-dilute suspensions: A numerical study, Med. Eng. Phys. **37**, 845 (2015).

[5] K. H. Jensen, W. Kim, N. M. Holbrook, and J. W. M. Bush, Optimal concentrations in transport systems, J. Roy. Soc. Int. **10**, 20130138 (2013).

[6] M. S. Hedrick, D. A. Duffield, and L. H. Cornell, Blood viscosity and optimal hematocrit in a deep-diving mammal, the northern elephant seal (*Mirounga angustirostris*), Can. J. Zool. **64**, 2081 (1986).

[7] O. Linderkamp, A. A. Stadler, and E. P. Zilow, Blood viscosity and optimal hematocrit in preterm and full-term neonates in 50- to 500-micrometer tubes, Ped. Res. **32**, 97 (1992).

[8] R. M. G. Wells, L. A. Beard, and G. C. Grigg, Blood viscosity and hematocrit in the estuarine crocodile, Crocodylus porosus, Comp. Biochem. Physiol. Part A: Physiol. **99**, 411 (1991).

[9] H. Stark and S. Schuster, Comparison of various approaches to calculating the optimal hematocrit in vertebrates, J. Appl. Physiol. **113**, 355 (2012).

[10] G. Birchard, Optimal hematocrit: Theory, regulation and implications, Am. Zool. **37**, 65 (1997).

[11] J. H. Barbee and G. R. Cokelet, Prediction of blood flow in tubes with diameters as small as 29 microns, Microvasc. Res. **3**, 17 (1971).
[12] H. H. Lipowsky, S. Usami, and S. Chien, In vivo measurements of "apparent viscosity" and microvessel hematocrit in the mesentery of the cat, Microvasc. Res. **19**, 297 (1980).
[13] A. P. Shepherd and G. L. Riedel, Optimal hematocrit for oxygenation of canine intestine, Circ. Res. **51**, 233 (1982).
[14] R. J. Phillips, R. C. Armstrong, R. A. Brown, A. L. Graham, and J. R. Abbott, A constitutive equation for concentrated suspensions that accounts for shear-induced particle migration, Phys. Fluids A: Fluid Dyn. **4**, 30 (1992).
[15] S. D. Hudson, Wall migration and shear-induced diffusion of fluid droplets in emulsions, Phys. Fluids **15**, 1106 (2003).
[16] D. Katanov, G. Gompper, and D. A. Fedosov, Microvascular blood flow resistance: Role of red blood cell migration and dispersion, Microvasc. Res. **99**, 57 (2015).
[17] R. G. Henríquez Rivera, X. Zhang, and M. D. Graham, Mechanistic theory of margination and flow-induced segregation in confined multicomponent suspensions: Simple shear and Poiseuille flows, Phys. Rev. Fluids **1**, 060501 (2016).
[18] Q. M. Qi and E. S. G. Shaqfeh, Theory to predict particle migration and margination in the pressure-driven channel flow of blood, Phys. Rev. Fluids **2**, 093102 (2017).
[19] R. Fåhraeus, The suspension stability of the blood, Physiol. Rev. **9**, 241 (1929).
[20] A. S. Popel and P. C. Johnson, Microcirculation and hemorheology, Annu. Rev. Fluid Mech. **37**, 43 (2005).
[21] J. O. Barber, J. P. Alberding, J. M. Restrepo, and T. W. Secomb, Simulated two-dimensional red blood cell motion, deformation, and partitioning in microvessel bifurcations, Ann. Biomech. Eng. **36**, 1690 (2008).
[22] V. Doyeux, T. Podgorski, S. Peponas, M. Ismail, and G. Coupier, Spheres in the vicinity of a bifurcation: Elucidating the Zweifach-Fung effect, J. Fluid Mech. **674**, 359 (2011).
[23] Z. Shen, G. Coupier, B. Kaoui, B. Polack, J. Harting, C. Misbah, and T. Podgorski, Inversion of hematocrit partition at microfluidic bifurcations, Microvasc. Res. **105**, 40 (2016).
[24] S. Roman, A. Merlo, P. Duru, F. Risso, and S. Lorthois, Going beyond 20 μm-sized channels for studying red blood cell phase separation in microfluidic bifurcations, Biomicrofluidics **10**, 034103 (2016).
[25] R. E. Klabunde, *Cardiovascular Physiology Concepts* (Lippincott Williams and Wilkins, Philadelphia, 2011).
[26] M. Abkarian, M. Faivre, R. Horton, K. Smistrup, C. A. Best-Popescu, and H. A. Stone, Cellular-scale hydrodynamics, Biomed. Mater. **3**, 034011 (2008).
[27] P. M. Vlahovska, T. Podgorski, and C. Misbah, Vesicles and red blood cells: From individual dynamics to rheology, C. R. Phys. **10**, 775 (2009).
[28] S. Guido and G. Tomaiuolo, Microconfined flow behavior of red blood cells in vitro, C. R. Phys. **10**, 751 (2009).
[29] D. Abreu, M. Levant, V. Steinberg, and U. Seifert, Fluid vesicles in flow, Adv. Coll. Int. Sci. **208**, 129 (2014).
[30] X. Li, P. M. Vlahovska, and G. E. Karniadakis, Continuum- and particle-based modeling of shapes and dynamics of red blood cells in health and disease, Soft Matter **9**, 28 (2013).
[31] M. Kraus, W. Wintz, U. Seifert, and R. Lipowsky, Fluid Vesicles in Shear Flow, Phys. Rev. Lett. **77**, 3685 (1996).
[32] I. Cantat and C. Misbah, Lift Force and Dynamical Unbinding of Adhering Vesicles Under Shear Flow, Phys. Rev. Lett. **83**, 880 (1999).
[33] C. Pozrikidis, Numerical simulation of cell motion in tube flow, Ann. Biomed. Eng. **33**, 165 (2005).
[34] P. Bagchi, Mesoscale simulation of blood flow in small vessels, Biophys. J. **92**, 1858 (2007).
[35] W. R. Dodson and P. Dimitrakopoulos, Spindles, Cusps, and Bifurcation for Capsules in Stokes Flow, Phys. Rev. Lett. **101**, 208102 (2008).
[36] E. Lac, A. Morel, and D. Barthès-Biesel, Hydrodynamic interaction between two identical capsules in simple shear flow, J. Fluid Mech. **573**, 149 (2007).

[37] S. K. Veerapaneni, D. Gueyffier, D. Zorin, and G. Biros, A boundary integral method for simulating the dynamics of inextensible vesicles suspended in a viscous fluid in 2D, J. Comput. Phys. **228**, 2334 (2009).
[38] D.-V. Le and Z. Tan, Large deformation of liquid capsules enclosed by thin shells immersed in the fluid, J. Comput. Phys. **229**, 4097 (2010).
[39] H. Zhao, A. H. G. Isfahani, L. N. Olson, and J. B. Freund, A spectral boundary integral method for flowing blood cells, J. Comput. Phys. **229**, 3726 (2010).
[40] G. Boedec, M. Leonetti, and M. Jaeger, 3D vesicle dynamics simulations with a linearly triangulated surface, J. Comput. Phys. **230**, 1020 (2011).
[41] D. Salac and M. Miksis, A level set projection model of lipid vesicles in general flows, J. Comput. Phys. **230**, 8192 (2011).
[42] Y. Kim and L.-C. Lai, Simulating the dynamics of inextensible vesicles by the penalty immersed boundary method, J. Comput. Phys. **229**, 4840 (2010).
[43] A. Farutin, T. Biben, and C. Misbah, 3D numerical simulations of vesicle and inextensible capsule dynamics, J. Comput. Phys. **275**, 539 (2014).
[44] H. Noguchi and G. Gompper, Shape transitions of fluid vesicles and red blood cells in capillary flows, Proc. Natl. Acad. Sci. USA **102**, 14159 (2005).
[45] M. M. Dupin, I. Halliday, C. M. Care, L. Alboul, and L. L. Munn, Modeling the flow of dense suspensions of deformable particles in three dimensions, Phys. Rev. E **75**, 066707 (2007).
[46] J. Clausen and C. K. Aidun, Capsule dynamics and rheology in shear flow: Particle pressure and normal stress, Phys. Fluid **22**, 123302 (2010).
[47] D. A. Fedosov, W. Pan, B. Caswell, G. Gompper, and G. E. Karniadakis, Predicting human blood viscosity *in silico*, Proc. Natl. Acad. Sci. USA **108**, 11772 (2011).
[48] B. Kaoui, J. Harting, and C. Misbah, Two-dimensional vesicle dynamics under shear flow: Effect of confinement, Phys. Rev. E **83**, 066319 (2011).
[49] T. Krüger, S. Frijters, F. Günther, B. Kaoui, and J. Harting, Numerical simulations of complex fluid-fluid interface dynamics, Eur. Phys. J.: Spec. Top. **222**, 177 (2013).
[50] I. V. Pivkin and G. E. Karniadakis, Accurate Coarse-Grained Modeling of Red Blood Cells, Phys. Rev. Lett. **101**, 118105 (2008).
[51] S. Chien, Red cell deformability and its relevance to blood flow, Annu. Rev. Physiol. **49**, 177 (1987).
[52] A. Pries, N. Neuhaus, and P. Gaehtgens, Blood viscosity in tube flow: Dependence on diameter and hematocrit, Am. J. Physiol.-Heart Circ. Physiol. **263**, H1770 (1992).
[53] A. R. Pries, T. W. Secomb, and P. Gaehtgens, Biophysical aspects of blood flow in the microvasculature, Cardiovasc. Res. **32**, 654 (1996).
[54] J. L. McWhirter, H. Noguchi, and G. Gompper, Flow-induced clustering and alignment of vesicles and red blood cells in microcapillaries, Proc. Natl. Acad. Sci. USA **106**, 6039 (2009).
[55] G. Tomaiuolo, L. Lanotte, G. Ghigliotti, C. Misbah, and S. Guido, Red blood cell clustering in Poiseuille microcapillary flow, Phys. Fluid **24**, 051903 (2012).
[56] P. Olla, The role of tank-treading motions in the transverse migration of a spheroidal vesicle in a shear flow, J. Phys. A: Math. Gen. **30**, 317 (1997).
[57] U. Seifert, Hydrodynamic Lift on Bound Vesicles, Phys. Rev. Lett. **83**, 876 (1999).
[58] T. M. Fischer, M. Stohr-Lissen, and H. Schmid-Schonbein, The red cell as a fluid droplet: Tank tread-like motion of the human erythrocyte membrane in shear flow, Science **202**, 894 (1978).
[59] J. Dupire, M. Socol, and A. Viallat, Full dynamics of a red blood cell in shear flow, Proc. Natl. Acad. Sci. USA **109**, 20808 (2012).
[60] X. Grandchamp, G. Coupier, A. Srivastav, C. Minetti, and T. Podgorski, Lift and Down-Gradient Shear-Induced Diffusion in Red Blood Cell Suspensions, Phys. Rev. Lett. **110**, 108101 (2013).
[61] L. Lanotte, J. Mauer, S. Mendez, D. A. Fedosov, J.-M. Fromental, V. Claveria, F. Nicoud, G. Gompper, and M. Abkarian, Red cells' dynamic morphologies govern blood shear thinning under microcirculatory flow conditions, Proc. Natl. Acad. Sci. USA **113**, 13289 (2016).
[62] Y. C. Fung, *Biomechanics: Circulation* (Springer, Berlin, 1997).

[63] T. Krüger, F. Varnik, and D. Raabe, Efficient and accurate simulations of deformable particles immersed in a fluid using a combined immersed boundary lattice Boltzmann finite element method, Comput. Method. Appl. **61**, 3485 (2011).
[64] S. Suresh, Mechanical response of human red blood cells in health and disease: Some structure-property-function relationships, J. Mater. Res. **21**, 1871 (2006).
[65] A. G. Koutsiaris, S. V. Tachmitzi, P. Papavasileiou, N. Batis, M. G. Kotoula, A. D. Giannoukas, and E. Tsironi, Blood velocity pulse quantification in the human conjunctival pre-capillary arterioles, Microvasc. Res. **80**, 202 (2010).
[66] O. Linderkamp, P. Y. K. Wu, and H. J. Meiselman, Geometry of neonatal and adult red blood cells, Pediatr. Res. **17**, 250 (1983).
[67] Y. C. Fung, *Biomechanics: Mechanical Properties of Living Tissues* (Springer, Berlin, 1993).
[68] D. Cordasco and P. Bagchi, Intermittency and synchronized motion of red blood cell dynamics in shear flow, J. Fluid Mech. **759**, 472 (2014).
[69] T. W. Secomb, Flow-dependent rheological properties of blood in capillaries, Microvasc Res. **34**, 46 (1987).
[70] G. R. Cokelet and H. L. Goldsmith, Decreased hydrodynamic resistance in the two-phase flow of blood through small vertical tubes at low flow rates, Circ. Res. **68**, 1 (1991).
[71] M. Sharan and A. S. Popel, A two-phase model for flow of blood in narrow tubes with increased effective viscosity near the wall, Biorheology **38**, 415 (2001).
[72] I. M. Krieger and T. J. Dougherty, A mechanism for non-Newtonian flow in suspensions of rigid spheres, Trans. Soc. Rheol. **3**, 137 (1959).
[73] D. A. Fedosov, B. Caswell, A. S. Popel, and G. E. Karniadakis, Blood flow and cell-free layer in microvessels, Microcirc. **17**, 615 (2010).
[74] F. R. Da Cunha and E. J. Hinch, Shear-induced dispersion in a dilute suspension of rough spheres, J. Fluid Mech. **309**, 211 (1996).
[75] P. Olla, The lift on a tank-treading ellipsoidal cell in a shear flow, J. Phys. II **7**, 1533 (1997).
[76] M. Abkarian, C. Lartigue, and A. Viallat, Tank Treading and Unbinding of Deformable Vesicles in Shear Flow: Determination of the Lift Force, Phys. Rev. Lett. **88**, 068103 (2002).
[77] G. Coupier, B. Kaoui, T. Podgorski, and C. Misbah, Noninertial lateral migration of vesicles in bounded Poiseuille flow, Phys. Fluids **20**, 111702 (2008).
[78] V. Vitkova, M.-A. Mader, B. Polack, C. Misbah, and T. Podgorski, Micro-macro link in rheology of erythrocyte and vesicle suspensions, Biophys. J. **95**, L33 (2008).
[79] N. Callens, C. Minetti, G. Coupier, M.-A. Mader, F. Dubois, C. Misbah, and T. Podgorski, Hydrodynamic lift of vesicles under shear flow in microgravity, Europhys. Lett. **83**, 24002 (2008).
[80] T. M. Fischer and R. Korzeniewski, Threshold shear stress for the transition between tumbling and tank-treading of red blood cells in shear flow: Dependence on the viscosity of the suspending medium, J. Fluid Mech. **736**, 351 (2013).
[81] L. Bureau, G. Coupier, F. Dubois, A. Duperray, A. Farutin, C. Minetti, C. Misbah, T. Podgorski, D. Tsvirkun, and M. Vysokikh, Blood flow and microgravity, C. R. Mécanique **345**, 78 (2017).
[82] G. Ghigliotti, T. Biben, and C. Misbah, Rheology of a dilute two-dimensional suspension of vesicles, J. Fluid Mech. **653**, 489 (2009).
[83] V. Vitkova, A. Farutin, B. Polack, C. Misbah, and T. Podgorski, Erythrocyte dynamics in flow affects blood rheology, J. Phys.: Conf. Ser. **398**, 012027 (2012).
[84] X. Troussard, S. Vol, E. Cornet, V. Bardet, J.-P. Couaillac, C. Fossat, J.-C. Luce, E. Maldonado, V. Siguret, J. Tichet, O. Lantieri, and J. Corberand, Etude des valeurs normales de l'hémogramme chez l'adulte: Un besoin pour une meilleure interprétation et pour l'accréditation du laboratoire, Ann. Biol. Clin. **72**, 561 (2014).
[85] C. G. Ellis, J. Jagger, and M. Sharpe, The microcirculation as a functional system, Critical Care **9**, S3 (2005).
[86] M. G. Newberry, D. B. Ennis, and V. M. Savage, Testing foundations of biological scaling theory using automated measurements of vascular networks, PLoS Comput. Biol. **11**, e1004455 (2015).

[87] C. D. Murray, The physiological principle of minimum work. I. The vascular system and the cost of blood volume, Proc. Natl. Acad. Sci. USA **12**, 207 (1926).
[88] R. Karshafian, P. N. Burns, and M. R. Henkelman, Transit time kinetics in ordered and disordered vascular trees, Phys. Med. Biol. **48**, 3225 (2003).
[89] S. K. Stamatelos, E. Kim, A. P. Pathak, and A. S. Popel, A bioimage informatics based reconstruction of breast tumor microvasculature with computational blood flow predictions, Microvasc. Res. **91**, 8 (2014).
[90] H. Rieger and M. Welter, Integrative models of vascular remodeling during tumor growth, Wiley Interdiscip. Rev.: Syst. Biol. Med. **7**, 113 (2015).
[91] M. Peyrounette, Y. Davit, M. Quintard, and S. Lorthois, Multiscale modelling of blood flow in cerebral microcirculation: Details at capillary scale control accuracy at the level of the cortex, PLoS One **13**, e0189474 (2018).
[92] K. H. Albrecht, P. Gaehtgens, A. Pries, and M. Heuser, The Fahraeus effect in narrow capillaries (id 3.3 to 11.0 μm), Microvasc. Res. **18**, 33 (1979).
[93] I. H. Sarelius and B. R. Duling, Direct measurement of microvessel hematocrit, red cell flux, velocity, and transit time, Am. J. Physiol.-Heart Circ. Physiol. **243**, H1018 (1982).
[94] B. Klitzman and B. R. Duling, Microvascular hematocrit and red cell flow in resting and contracting striated muscle, Am. J. Physiol.-Heart Circ. Physiol. **237**, H481 (1979).
[95] A. R. Pries, T. W. Secomb, P. Gaehtgens, and J. F. Gross, Blood flow in microvascular networks. experiments and simulation, Circ. Res. **67**, 826 (1990).